Multiple period *s-p* hybridization in nano-strip embedded photonic crystal

Seunghoon Han, Il-Min Lee, Hwi Kim, and Byoungho Lee

School of Electrical Engineering, Seoul National University, Seoul 151-744, Korea
Phone: +82-2-880-7245, Fax: +82-2-873-9953
byoungho@snu.ac.kr

http://oeqelab.snu.ac.kr

Abstract: We report and analyze hybridization of *s*-state and *p*-state modes in photonic crystal one-dimensional defect cavity array. When embedding a nano-strip into a dielectric rod photonic crystal, an effective cavity array is made, where each cavity possesses two cavity modes: *s*-state and *p*-state. The two modes are laterally even versus the nano-strip direction, and interact with each other, producing defect bands, of which the group velocity becomes zero within the first Brillouin zone. We could model and describe the phenomena by using the tight-binding method, well agreeing with the plane-wave expansion method analysis. We note that the reported *s*- and *p*-state mode interaction corresponds to the hybridization of atomic orbital in solid-state physics. The concept of multiple period *s-p* hybridization and the proposed model can be useful for analyzing and developing novel photonic crystal waveguides and devices.

OCIS codes: (130.2790) Guided waves, (230.5750) Resonators, (230.7370) Waveguides

References and links

1. A. Chutinan and S. Noda, “Waveguides and waveguide bends in two-dimensional photonic crystal slabs,” Phys. Rev. B **62**, 4488-4492 (2000).
2. S. G. Johnson, P. R. Villeneuve, S. Fan, and J. D. Joannopoulos, “Linear waveguides in photonic-crystal slabs,” Phys. Rev. B **62**, 8212-8222 (2000).
3. N. Stefanou and A. Modinos, “Impurity bands in photonic insulators,” Phys. Rev. B **57**, 12127-12133 (1998).
4. A. Yariv, Y. Xu, R. K. Lee, and A. Scherer, “Coupled-resonator optical waveguide: a proposal and analysis,” Opt. Lett. **24**, 711-713 (1999).
5. Y. Xu, R. K. Lee, and A. Yariv, “Propagation and second-harmonic generation of electromagnetic waves in a coupled-resonator optical waveguide,” J. Opt. Soc. Am. B **17**, 387-400 (2000).
6. E. Ozbay, M. Bayindir, I. Bulu, and E. Cubukcu, “Investigation of localized coupled-cavity modes in two-dimensional photonic bandgap structures,” IEEE J. Quantum Electron. **38**, 837-843 (2002).
7. M. Notomi, K. Yamada, A. Shinya, J. Takahashi, C. Takahashi, and I. Yokohama, “Extremely large group-velocity dispersion of line-defect waveguides in photonic crystal slabs,” Phys. Rev. Lett. **87**, 253902 (2001).
8. M. Lončar, J. Vučković, and A. Scherer, “Methods for controlling positions of guided modes of photonic-crystal waveguides,” J. Opt. Soc. Am. B **18**, 1362-1368 (2001).
9. D. Mori and T. Baba, “Dispersion-controlled optical group delay device by chirped photonic crystal waveguides,” Appl. Phys. Lett. **85**, 1101-1103 (2004).
10. A. Y. Petrov and M. Eich, “Zero dispersion at small group velocities in photonic crystal waveguides,” Appl. Phys. Lett. **85**, 4866-4868 (2004).
11. L. Brillouin, *Wave Propagation in Periodic Structures 2nd ed.* (Dover Publications, New York, 1953).
12. N. W. Ashcroft and N. D. Mermin, *Solid State Physics* (Saunders College Publishing, Philadelphia, 1976).
13. E. Lidorikis, M. M. Sigalas, E. N. Economou, and C. M. Soukoulis, “Tight-binding parametrization for photonic band gap materials,” Phys. Rev. Lett. **81**, 1405-1408 (1998).
14. J. P. Albert, C. Jouanin, D. Cassagne, and D. Bertho, “Generalized Wannier function method for photonic crystals,” Phys. Rev. B **61**, 4381-4384 (2000).

Received 22 February 2005; revised 26 March 2005; accepted 28 March 2005

15. D. Leuenberger, R. Ferrini, and R. Houdré, "An *initio* tight-binding approach to photonic-crystal based coupled cavity waveguides," J. Appl. Phys. 95, 806-809 (2004).
16. V. Yannopapas, A. Modinos, and N. Stefanou, "Optical properties of metallodielectric photonic crystals," Phys. Rev. B **60**, 5359-5365 (1999).
17. V. Yannopapas, A. Modinos, and N. Stefanou, "Waveguides of defect chains in photonic crystals," Phys. Rev. B **65**, 235201 (2002).
18. W. A. Harrison, *Electronic Structure and the Properties of Solids* (Freeman, San Francisco, 1980).
19. S. T. Pantelides and W. A. Harrison, "Structure of the valence bands of zinc-blende-type semiconductors," Phys. Rev. B **11**, 3006-3021 (1975).
20. W. T. Lau and S. Fan, "Creating large bandwidth line defects by embedding dielectric waveguides into photonic crystal slabs," Appl. Phys. Lett. **81**, 3915-3917 (2002).
21. K. Sakoda, *Optical Properties of Photonic Crystals* (Springer-Verlag, New York, 2001).
22. The PWE simulations were carried out with BandSOLVE commercial software by RSoft Design Group.
23. J. D. Joannopoulos, R. D. Meade, and J. N. Winn, *Photonic Crystals* (Princeton U. Press, Princeton, 1995).
24. B. E. A. Saleh and M. C. Teich, *Fundamentals of Photonics* (John Wiley & Sons, New York, 1991).
25. S. Akiba, M. Usami, and K. Utaka, "1.5-μm λ/4-shifted InGaAsP/InP DFB lasers," J. Lightwave Technol. **LT-5**, 1564-1573 (1987).
26. X. Checoury, P. Boucaud, J-M. Lourtioz, F. Pommereau, C. Cuisin, E. Derouin, O. Drisse, L. Legouezigou, F. Lelarge, F. Poingt, G. H. Duan, D. Mulin, S. Bonnefont, O. Gauthier-Lafaye, J. Valentin, F. Lozes, and A. Talneau, "Distributed feedback regime of photonic crystal waveguide lasers at 1.5 μm," Appl. Phys. Lett. **85**, 5502-5504 (2004).

1. Introduction

Photonic crystal waveguides have inherent advantages in photonic integrated circuits (e.g., photonic band gap (PBG) confinement of optical wave, small group velocity and group velocity dispersions different from those of the conventional waveguides) and have been researched actively using various concepts for novel applications. Practical slab waveguide structures were reported analyzing the height confinement effect of the slab structure [1, 2]. In addition, a coupled-resonator optical waveguide (CROW), which uses the peculiar weak-coupling characteristics of photonic crystal resonators, was proposed, facilitating a great many applications [3-6]. For certain types of photonic crystal waveguides, it was found that multiple waveguide defect bands can occur with multi-mode characteristics, large group velocity dispersion and zero-group velocity inside the first Brillouin zone [7, 8]. Many research studies have been performed for analyzing and exploiting their defect band characteristics, such as controlling the guided mode frequencies and dispersion characteristics for device applications [8-10]. However, we note that although some physical interpretation was made of such structures [6, 7, 10], theoretical modeling providing physical insights to the photonic interactions for the corresponding defect band dispersions has not been well established.

We found that similar multi-mode/multi-band defect bands occur in the nano-strip embedded photonic crystal (NEPC), where a nano-strip causes one-dimensional defect inside a dielectric rod photonic crystal. In this paper, we attempt to show and model such phenomena as photonic correspondence of the atomic orbital hybridization over multiple periods in solid-state physics. Similar to the general wave propagation within periodic structures and electron propagation in the solid-crystals [11, 12], the NEPC defect bands become a photonic version of multiple period *s*-*p* state hybridization. In the NEPC, photonic *s*- and *p*-state cavity modes are interacting with each other over the multiple periods in the propagation direction. This interaction can be described by the tight-binding method with multiples of resonating modes [3, 5, 13-15]. Actually, it was reported that in photonic crystal, any finite number of cavity modes could interact with one another under the tight-binding method description [15]. It was also predicted that in certain cases cavity mode interactions up to the second-nearest neighbors might occur.

What we show in this paper is the existence and tight-binding method description of such phenomena realized in NEPC as multiple period *s*-*p* hybridization. The *s*-*p* hybridization occurs between laterally even modes versus the propagation direction (i.e., nano-strip direction), which should be distinguished from the even and odd mode interaction as in [5] and [7]. This hybridization and its tight-binding approach description can be useful for design and analysis of novel waveguide and photonic device development. We note that similar phenomena in photonic crystals have been found, such as in the cases of the metallodielectric photonic crystals [16] and also for the defect chains in the three-dimensional photonic crystal [17]. In the electronic solid-state case, similar multiple period interactions of atomic orbital can also be found [18, 19]. Similar to our NEPC structure, dielectric waveguide embedding in photonic crystal has previously been proposed [20]. However, in [20], the authors aimed at obtaining single-mode bands with large bandwidth by embedding relatively large dielectric waveguide compared to our NEPC nano-strip. In this case, we note that the hybridization of cavity modes does not occur, since well-localized cavity modes are not well defined. This is manifested in the resulting defect band dispersions, whereas in [20], the dispersion is low and, on the contrary, in our case it was quite large. In the following analysis, to simplify the problem we consider the NEPC as a two-dimensional structure. However, for a three-dimensional slab-structure, similar generalization may be possible, including vertical symmetry mode effect and light line slab guiding limitations [21].

2. NEPC: effective defect cavity array with *s* and *p* cavity modes

Figure 1 shows the NEPC's structure (Fig. 1(a)) and its band dispersion characteristics (Fig. 1(b), i.e., its projected band diagram). The NEPC is obtained by embedding a nano-strip within a dielectric-rod/air-background photonic crystal, shown as a horizontal red line in Fig. 1(a). By embedding this nano-strip, a high index defect waveguide is made, causing two defect bands to come down from the upper air band, as seen in Fig. 1(b). For the following analysis, GaAs with a refractive index of 3.4 was assumed for the dielectric material of the photonic crystal rod and nano-strip. Rod diameter and nano-strip width were 0.4a and 0.1a, respectively, where a is the period of the photonic crystal structure. The band diagram was obtained using plane wave expansion (PWE) calculation with 8 by 1 (x by z direction) supercell method [22]. In the calculation, electromagnetic variational theorem [23] was used with iterative minimization techniques. The band diagram of Fig. 1(b) is for the case of TM polarization, in which only y-directional electric field exists. Within the PBG, the two defect bands become waveguide bands with multi-mode characteristics for certain frequencies and zero group velocity away from the Brillouin zone edge (i.e., near normalized frequency 0.34). However, for the upper defect band (blue line in Fig. 1(b)), the low wave vector part goes into the upper air band so that large loss occurs due to interactions with the air band extended modes. Although this is an artificial structure to analyze and interpret the hybridization, actual realization of the hybridized band structure may use some lower index background even with three-dimensional slab structure [2]. Figure 1(c) shows a conceptual interpretation of the NEPC as an effective defect cavity one-dimensional array with period a. This interpretation forms the basis of the theoretical modeling in the following section.

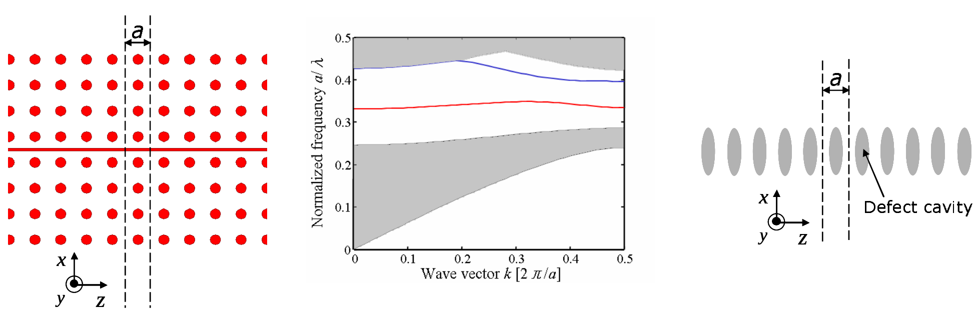

Fig. 1. Two-dimensional NEPC: (a) dielectric rod photonic crystal with nano-strip embedding, (b) projected band diagram, red and blue lines: NEPC defect bands, (c) conceptual interpretation of NEPC: one-dimensional defect cavity array.

#6648 - $15.00 US Received 22 February 2005; revised 26 March 2005; accepted 28 March 2005

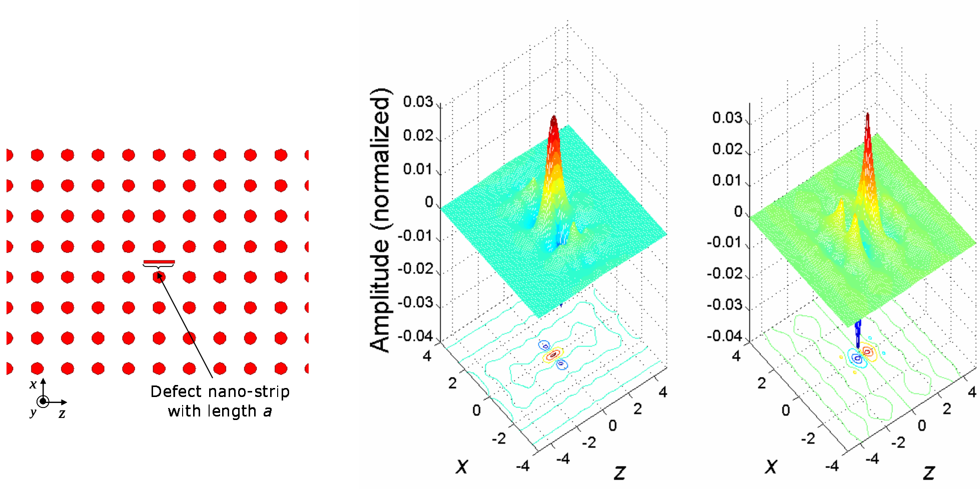

(a) (b) (c)

Fig. 2. Effective defect cavity of NEPC: (a) elementary effective defect cavity, (b) *s*-state cavity mode field distribution, (c) *p*-state cavity mode field distribution.

The characteristics of the NEPC effective defect cavity are shown in Fig. 2. A portion of the nano-strip interacting with two adjacent dielectric rods forms an effective defect cavity within each period along the nano-strip direction. In Fig. 2(a), one elementary effective defect cavity is shown to be made by embedding a nano-strip with length *a*. The NEPC structure of Fig. 1(a) is considered to be composed of elementary defect nano-strips, like Fig. 2(a), forming an effective cavity array, as seen in Fig. 1(c). By using the PWE calculation with 8 by 10 (x by z) supercell method for the defect cavity of Fig. 2(a), we could find that there are two cavity modes with field distribution, as plotted in Figs. 2(b) and 2(c). With respect to the one-dimensional periodicity along the defect cavity array direction, we can see that each mode corresponds to the *s*-state (Fig. 2(b), normalized resonant frequency 0.354) and *p*-state (Fig. 2(c), normalized resonant frequency 0.385) similar to the atomic crystal orbital states [2]. We note that field confinement along the nano-strip direction mainly originated from the PBG reflection effect rather than from the Fresnel reflection at the nano-strip defect ends. Since nano-strip width is much smaller than the resonating optical wavelength (i.e., about 30 times smaller), the nano-strip can only support fundamental guiding mode [24]. For this guiding mode, most field energy should distribute outside the nano-strip as an evanescent field. This field distribution can also be observed in the PWE calculation of Fig. 2(b) and 2(c). This means that in the NEPC structure, a wave propagating along the nano-strip feels the PBG mirror at every period and bounces back and forth within each period along the nano-strip direction. This supports our assumption of the effective defect cavity array to be appropriate.

3. Tight-binding model: multiple period *s-p* hybridization

For the description of the defect cavity array, we use a tight-binding method with multiple cavity modes. We follow the general approach described in [4] and [5] for the hybridization in NEPC and explain the physical characteristics from the model. According to the tight-binding approximation, when the coupling between the adjacent cavity modes is sufficiently weak to maintain each cavity resonance at each lattice site but, induces corrections to the isolated cavities, we can take the defect band of the coupled-cavity array as linear combination of the cavity modes. Specifically,

$$\vec{E}_k(\vec{r},t)=\exp(i\omega_k t)\sum_n \exp(-inka)\sum_l A_l \vec{E}_{\Omega_l}(\vec{r}-na\hat{e}_z). \tag{1}$$

Here a is the period along the cavity array direction, A_l and $\vec{E}_{\Omega_l}$ are relative amplitude for each elementary cavity mode, l, and its resonating mode profile (i.e., s and p modes), and n is an integer for multiple period interaction. Since the cavity array is periodic along its direction, the defect band mode also becomes Bloch wave, where we can consider only the first Brillouin zone of the wave vector k (i.e., $-\pi/a \le k \le \pi/a$) in characterizing its band dispersion.

Then, $\vec{E}_k(\vec{r},t)$ satisfies the Maxwell equations, as

$$\vec{\nabla}\times\vec{\nabla}\times\vec{E}_k=\varepsilon(\vec{r})\frac{\omega_k^2}{c^2}\vec{E}_k \tag{2}$$

where $\varepsilon(\vec{r})$ is the dielectric constant of the NEPC system and ω_k is the waveguide mode eigenfrequency. In the same way, $\vec{E}_{\Omega_l}$ satisfies Eq. (2), where $\varepsilon(\vec{r})$ is replaced by $\varepsilon_o(\vec{r})$, the effective defect cavity dielectric profile, and ω_k is replaced with Ω_l, the resonance frequency of the effective cavity. We take orthonormal condition to the cavity modes as

$$\int d\vec{r}\,\varepsilon_o(\vec{r})\vec{E}_{\Omega_l}(\vec{r})\cdot\vec{E}_{\Omega_m}(\vec{r})=\delta_{l,m}, \tag{3}$$

where we consider $\vec{E}_{\Omega_l}$ to be real.

After inserting Eq. (1) into Eq. (2), multiplying both sides from the left by $\vec{E}_{\Omega_m}(\vec{r})$ (m's for s- and p-state) and spatially integrating, we can get two eigen equations for the mode amplitudes as

$$\sum_l A_l\Omega_l^2\left[\delta_{m,l}+\sum_{n\neq 0}\exp(-inka)\beta_{m,l}^n\right]=\omega_k^2\sum_l A_l\left[\delta_{m,l}+\Delta\alpha_{m,l}+\sum_{n\neq 0}\exp(-inka)\alpha_{m,l}^n\right] \tag{4}$$

where $\alpha_{m,l}^n$, $\beta_{m,l}^n$, and $\Delta\alpha_{m,l}$ are defined as

$$\alpha_{m,l}^n=\int d\vec{r}\,\varepsilon(\vec{r})\vec{E}_{\Omega_m}(\vec{r})\cdot\vec{E}_{\Omega_l}(\vec{r}-na\hat{e}_z), \tag{5a}$$

$$\beta_{m,l}^n=\int d\vec{r}\,\varepsilon_o(\vec{r}-na\hat{e}_z)\vec{E}_{\Omega_m}(\vec{r})\cdot\vec{E}_{\Omega_l}(\vec{r}-na\hat{e}_z), \tag{5b}$$

$$\Delta\alpha_{m,l}=\int d\vec{r}\left[\varepsilon(\vec{r})-\varepsilon_o(\vec{r})\right]\vec{E}_{\Omega_m}(\vec{r})\cdot\vec{E}_{\Omega_l}(\vec{r}). \tag{5c}$$

We note that due to the symmetry of the p-state cavity mode along the defect cavity array direction (i.e., z-direction), the symmetry relations of the parameters of Eq. (5a) and (5b) become $\alpha_{a,b}^n=-\alpha_{a,b}^{-n}$, $\beta_{a,b}^n=-\beta_{a,b}^{-n}$ different from the cases of $\alpha_{a,a}^n=\alpha_{a,a}^{-n}$, $\alpha_{b,b}^n=\alpha_{b,b}^{-n}$, $\beta_{a,a}^n=\beta_{a,a}^{-n}$, and $\beta_{b,b}^n=\beta_{b,b}^{-n}$. Considering this, Eq. (4) becomes

$$\begin{aligned}&A_m\left[-\omega_k^2\left\{1+\Delta\alpha_{m,m}+\sum_{n\neq 0}2\alpha_{m,m}^n\cos(nka)\right\}+\Omega_m^2\left\{1+\sum_{n\neq 0}2\beta_{m,m}^n\cos(nka)\right\}\right]\\&\quad-iA_l\left[-\omega_k^2\sum_{n\neq 0}2\alpha_{m,l}^n\sin(nka)+\Omega_l^2\sum_{n\neq 0}2\beta_{m,l}^n\sin(nka)\right]=0,\end{aligned} \tag{6}$$

#6648 - $15.00 US Received 22 February 2005; revised 26 March 2005; accepted 28 March 2005

where, m and l denote different cavity mode states, respectively. Equation (6) can have nontrivial solution when its determinant becomes zero, which gives amplitude ratio between A_s and A_p, and the band dispersion relations.

From this condition, we know that the two resulting defect bands of the coupled defect cavity array have some interesting characteristics, such that at the Brillouin edge and zero wave vector, only one cavity mode vibrates and, in the intermediate wave vector region, the two cavity modes vibrate with 90-degree relative phase difference. We note that for the multiple period interaction, we can also define a coupling factor $\kappa_{m,l}^{n}$ like

$$\begin{aligned}\kappa_{m,l}^{n} &= \beta_{m,l}^{n} - \alpha_{m,l}^{n} \\ &= \int d\vec{r}\left[\varepsilon_o(\vec{r} - na\hat{e}_z) - \varepsilon(\vec{r} - na\hat{e}_z)\right]\vec{E}_{\Omega_m}(\vec{r}) \cdot \vec{E}_{\Omega_l}(\vec{r} - na\hat{e}_z)\end{aligned} \tag{7}$$

to estimate the weak coupling between cavity modes, which are multiple period distant from each other.

4. Numerical analysis : tight-binding model and PWE analysis

Figure 3 shows comparison of the NEPC band dispersion calculation between the PWE method (numerically stable [15]) and the proposed tight-binding model for the multiple period *s*-*p* hybridization. We can see that by increasing the interaction lengths from just the nearest neighbors (Fig. 3(a)) to the fourth-nearest neighbors (Fig. 3(c)), the proposed model correctly converges to the PWE results. This means that the defect bands of the NEPC comes from the *s*- and *p*-state cavity mode interactions over up to the fourth-nearest neighbors. For the upper defect band (blue in Fig. 3(c)) with low wave vector, there occurs large deviation of the proposed model from the PWE calculation. This is due to the coupling between the upper *s*-*p* hybridized band mode and the extended band modes of the air band (Fig. 1(b)), where the two-cavity modes assumption of the proposed model is not satisfied. Figure 4 is a contour map of the mode profiles of the two defect bands. Mode profiles in 8 by 1 (x by z) unit area are obtained using the proposed tight-binding model as well as the PWE calculation. We can see the results of the two methods to be agreeing well with each other, although in the vicinity of the air band, the upper defect band mode does not match the PWE result (i.e., Fig. 4(a) and (b) upper contours). In Fig. 5, the relative amplitudes of the two cavity modes in each defect band are plotted. These amplitudes were normalized as $\left|A_s\right|^2 + \left|A_p\right|^2 = 1$. We can see that at the Brillouin zone edges and the zero wave vector, only one cavity mode vibrates and the amplitude is monotonically decreasing or increasing in the intermediate wave vector regions. This hybridization of the *s*- and *p*-state modes originates from the relationship of the coefficients $\alpha_{m,l}^{n}$'s and $\beta_{m,l}^{n}$'s, and cavity resonance frequencies Ω_l's. From Eq. (6), we can see that at the zero wave vector and at the Brillouin zone edge, only one cavity mode vibrates for each band. Generally, when the coefficients and cavity resonance frequency relationship induces relative frequency change for the two vibrating cavity modes at these two wave vectors, the *s*- and *p*-state hybridization occurs over the Brillouin zone wave vectors. We also note that at the Brillouin zone edge, the two bands can support two lasing modes if we consider fabricating distributed feedback (DFB) laser. The *p*-state mode for the lower frequency and the *s*-state mode for the higher frequency of the NEPC case (i.e., Fig. 4(d)), correspond to the lasing modes of the uniform corrugated DFB laser [25]. Actually, fabrication of the photonic crystal DFB laser with optical pumping was recently reported using similar band structures [26]. In this laser scheme, multi-quantum well structure was introduced into the photonic crystal slab waveguide. In photonic crystal DFB lasers, like in [26], we can expect that the overlap area of each mode profile relative to the active region will affect the optical gain of each mode.

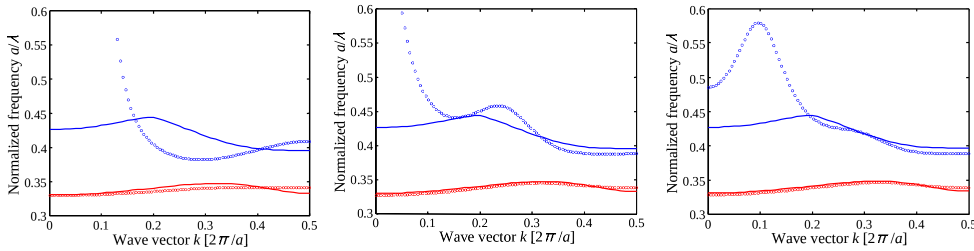

(a) (b) (c)

Fig. 3. Multiple period *s-p* hybridization in NEPC: solid lines; PWE results, circles; tight-binding model results for (a) nearest neighbor interaction only, (b) up to third-nearest neighbor interactions, (c) up to fourth-nearest neighbor interactions.

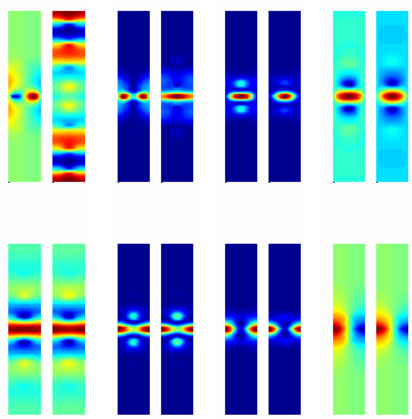

(a) (b) (c) (d)

Fig. 4. Mode profiles for (a) k = 0 (amplitude), (b) k = 0.25 (intensity), (c) k = 0.4 (intensity), (d) k = 0.5 (amplitude), left side; tight-binding model, right side; PWE analysis, upper side; upper band mode, lower side; lower band mode.

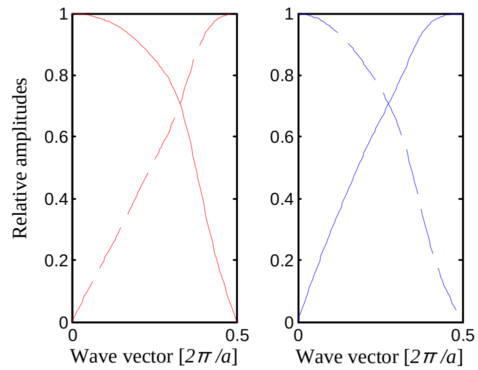

(a) (b)

Fig. 5. Relative amplitudes of the *s*-state (solid line) and *p*-state (dashed line) cavity modes for (a) lower defect band, (b) upper defect band.

Figure 6 shows convergence of the proposed tight-binding method (red, up to fourth nearest neighbor interactions) to the PWE calculation (blue line) for the lower defect band. The red dashed line in Fig. 6 is for the case in which the effective defect cavity is only a length, *a*, of the nano-strip, as in Fig. 2(a). Note that there are some deviations from the PWE calculation (blue line in Fig. 6). However, when we increase the nano-strip length of the effective defect cavity to 1.2*a* (red crosses) and then increase the refractive index of the strip to 3.9 (red circles), we can see that the tight-binding approach converges more well to the PWE calculation result. It means that for the optical field confinement along the propagation direction (i.e., *z* direction in Fig. 2(a)) in each cavity, the nano-strip waveguiding effect needs to be considered, to some extent, differently from the simple cavity model of Fig. 2(a), based on just the PBG reflection effect. However, with some clever cavity structures or theoretical method development for the real effective cavity, we are expecting that practical application of the multiple period *s-p* hybridization might be possible. In relation to the weak coupling condition of the tight-binding method, we note that the coupling factors (i.e., $\kappa_{m,l}^{n}$ in Eq. (7)) for the effective cavity model of red circles in Fig. 6, are of the order 10^{-2} or less for all the multiple period interactions. For this cavity model, Fig. 7 shows comparison of the guiding mode profiles (for 8 by 1 (x by z) unit area) between the tight-binding model and PWE calculation. We can see that the proposed model's results agree very well with the PWE field results.

#6648 - $15.00 US Received 22 February 2005; revised 26 March 2005; accepted 28 March 2005

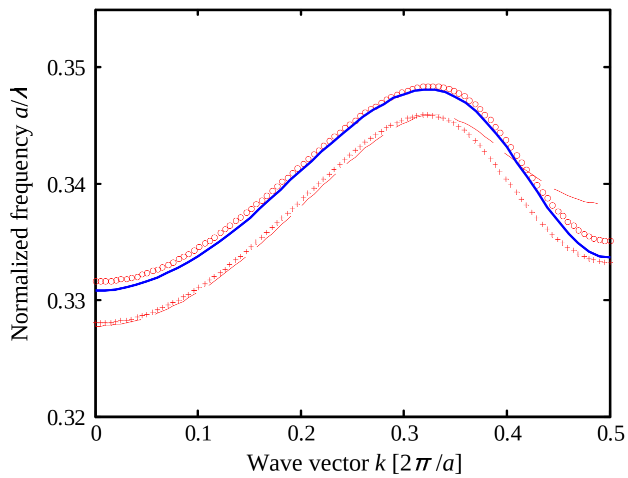

Fig. 6. Effective cavity fitting for tight-binding model convergence to the PWE method: blue line; PWE method, red dashed line; tight-binding method (nano-strip with length of *a*), red crosses; tight-binding method (nano-strip with increased length of 1.2*a*), red circles; tight-binding method (nano-strip with increased length of 1.2*a* and increased refractive index of 3.9).

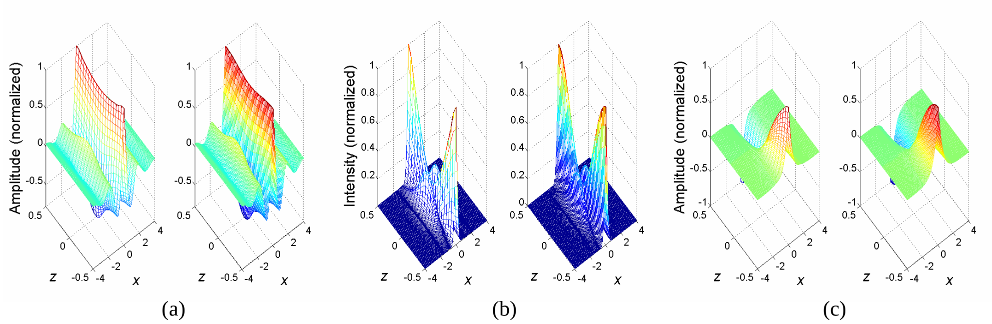

Fig. 7. Mode field profile comparison for (a) k = 0 (amplitude), (b) k = 0.32 (intensity), (c) k = 0.5 (amplitude), left side; tight-binding model, right side; the PWE method.

5. Conclusion

This paper has found and shown the existence of the multiple period *s-p* hybridization in the case of photonic crystal. This phenomenon is possible in NEPC structure, where the embedded nano-strip forms an effective defect cavity array along its direction. Using the tight-binding method, we could analyze and describe the characteristics of the hybridized bands that agree well with the PWE calculations. We note that the proposed multiple period hybridization is a novel concept in photonic crystal one-dimensional defects, which is distinguished from other defects like CROW (i.e., nearest neighbor interaction) and conventional waveguides (i.e., long range interaction). Although the phenomena were considered only in NEPC structure, by developing some clever structures or theoretical methods for design (e.g., effective cavity defining method), various applications will be possible from waveguides to photonic devices.

#6648 - $15.00 US Received 22 February 2005; revised 26 March 2005; accepted 28 March 2005